Inorganic Chemistry
Article

Inorg. Chem. **2009**, *48*, 9623–9630 **9623**
DOI: 10.1021/ic900090e

Observation of Magnetic Bistability in Polymorphs of the $[Ni(dmit)_2]^-$ Complexes

Shuangquan Zang,[†,∥] Xiaoming Ren,[†] Yang Su,[†] You Song,[†] Wenjun Tong,[†] Zhaoping Ni,[†] Hanhua Zhao,[‡] Song Gao,[§] and Qingjin Meng*[,†]

[†]*State Key Laboratory of Coordination Chemistry, Department of Chemistry, Nanjing University, Nanjing 210093, P. R. China,* [‡]*Department of Chemistry, Texas A&M University, P.O. Box 30012, College Station, Texas 77842-3012, and* [§]*State Key Laboratory of Rare Earth Materials Chemistry and Applications, College of Chemistry and Molecular Engineering, Peking University, Beijing 100871, P. R. China.* [∥]*Current address: Department of Chemistry, Zhengzhou University, Zhengzhou 450000, Henan, P. R. China.*

Received January 16, 2009

Four ion-pair complexes of $[Ni(dmit)_2]^-$ with $[NO_2bzql]^+$ have been obtained, which belong to two kinds of polymorph forms, $[NO_2bzql][Ni(dmit)_2]$ (**1**α and **1**β) and $[NO_2bzql][Ni(dmit)_2]\cdot CH_3COCH_3$ (**2**α and **2**β) (where dmit = 2-thioxo-1,3-dithiole-4,5-dithiolate and $[NO_2bzql]^+$ = 1-(4-nitrobenzyl)quinolinium). Though **1**α, **2**α, and **2**β all show anionic dimerization structures at room temperature, they have different anionic and cationic arrangement fashions, which give rise to different magnetic behaviors for these polymorphs or pseudo-polymorphs. Compounds **1**α, **1**β, and **2**α exhibit magnetic bistabilities. In particular, **1**α has a hysteretic loop at ~55 K, while **2**β does not display a spin transition in the 2−300 K range. On the basis of the crystal structure data of **2**α in high- and low-temperature phases, the magnetic coupling feature within the $[Ni(dmit)_2]^-$ spin dimer was explored with the broken-symmetry approach at the UBPW91/LANL2DZ level; combined with the experimental data and theoretical analyses, the relationship between the magnetic coupling nature and the stacking pattern of $[Ni(dmit)_2]^-$ anions as well as the origin of the phase interconversion are discussed.

Introduction

Molecular spin bistability materials have aroused a great deal of attention owing to their potential applications in many technical fields, such as magneto-thermal switching, information storage, and other molecular electronic devices.[1] The most well-known example of these materials is transition metal spin-crossover (SC) complexes.[1−4] Additionally, new bistability systems, such as charge transfer complexes,[5,6] valence ordering compounds,[7] and pure organic radical compounds,[8−10] have been developed.

*To whom correspondence should be addressed. E-mail: mengqj@nju.edu.cn.

(1) (a) Kahn, J. P.; Launary *Chemtronics* **1988**, *3*, 140–151. (b) Kahn, O. *Molecular Magnetism*; VCH: Weinheim, Germany, 1993. (c) Kahn, O.; Kröber, J.; Jay, C. *Adv. Mater.* **1992**, *4*, 718–728. (d) Gütlich, P.; Garcia, Y.; Woike, T. *Coord. Chem. Rev.* **2001**, *219−221*, 839–879. (e) Miller, J. S.; Drillon, M. *Magnetism: Molecules to Materials IV*; Wiley-VCH: Weinheim, Germany, 2003. (f) Bousseksou, A.; Molnár, G.; Matouzenko, G. *Eur. J. Inorg. Chem.* **2004**, 4353–4369. (g) Létard, J. F.; Guionneau, P.; Goux-Capes, L. *Top. Curr. Chem.* **2004**, *235*, 221–249.

(2) (a) Gütlich, P.; Hauser, A.; Spiering, H. *Angew. Chem.* **1994**, *106*, 2109–2141. Gütlich, P.; Hauser, A.; Spiering, H. *Angew. Chem., Int. Ed.* **1994**, *33*, 2024–2054. (b) Real, J. A.; Andrés, E.; Munoz, M. C.; Julve, M.; Granier, T.; Bousseksou, A.; Varret, F. *Science* **1995**, *268*, 265–267. (c) Kahn, O.; Martinez, C. J. *Science* **1998**, *279*, 44–48. (d) Real, J. A.; Gaspar, A. B.; Niel, V.; Muoz, M. C. *Coord. Chem. Rev.* **2003**, *236*, 121–141. (e) Gütlich, P.; Garcia, Y.; Goodwin, H. A. *Chem. Soc. Rev.* **2000**, *29*, 419–423.

(3) (a) Niel, V.; Thompson, A. L.; Muñoz, M. C.; Galet, A.; Goeta, A. E.; Real, J. A. *Angew. Chem., Int. Ed.* **2003**, *42*, 3760–3763. (b) Ksenofontov, V.; Gaspar, A. B.; Niel, V.; Reiman, S.; Real, J. A.; Gütlich, P. *Chem.—Eur. J.* **2004**, *10*, 1291–1298. (c) Reger, D. L.; Gardinier, J. R.; Gemmill, W. R.; Smith, M. D.; Shahin, A. M.; Long, G. J.; Rebbouh, L.; Grandjean, F. *J. Am. Chem. Soc.* **2005**, *127*, 2303–2316.

(4) (a) Takahashi, K.; Kawakami, T.; Gu, Z. Z.; Einaga, Y.; Ujishima, A.; Sato, O. *Chem. Commun.* **2003**, 2374–2375. (b) Dorbes, S.; Valade, L.; Real, J. A.; Faulmann, C. *Chem. Commun.* **2005**, 69–71. (c) Faulmann, C.; Orbes, S.; de Bonneval, B. G.; Molnár, G.; Bousseksou, A.; Gomez-Garcia, C. J.; Coronado, E.; Valade, L. *Eur. J. Inorg. Chem.* **2005**, 3261–3270.

(5) (a) Sato, O.; Iyoda, T.; Fujishima, A.; Hashimoto, K. *Science* **1996**, *272*, 704–705. (b) Shimamoto, N.; Ohkoshi, S.; Sato, O.; Hashimoto, K. *Inorg. Chem.* **2002**, *41*, 678–684. (c) Berlinguette, C. P.; Dragulescu-Andrasi, A.; Sieber, A.; Galán-Mascarós, J. R.; Güdel, H. U.; Achim, C.; Dunbar, K. R. *J. Am. Chem. Soc.* **2004**, *126*, 6222–6223. (d) Umezono, Y.; Fujita, W.; Awaga, K. *J. Am. Chem. Soc.* **2006**, *128*, 1084–1085. (e) Sato, O.; Tao, J.; Zhang, Y.-Z. *Angew. Chem., Int. Ed.* **2007**, *46*, 2152–2187.

(6) (a) Li, D.; Clérac, R.; Roubeau, O.; Harté, E.; Mathonière, C.; Bris, R. L.; Holmes, S. M. *J. Am. Chem. Soc.* **2008**, *130*, 252–258. (b) Kiriya, D.; Chang, H.; Kitagawa, S. *J. Am. Chem. Soc.* **2008**, *130*, 5515–5522. (c) Ohkoshi, S.-I.; Hamada, Y.; Matsuda, T.; Tsunobuchi, Y.; Tokoro, H. *Chem. Mater.* **2008**, *20*, 3048–3054.

(7) (a) Nakamura, T. *J. Phys. Soc. Jpn.* **2003**, *72*, 213–216. (b) Kojima, N.; Aoki, W.; Itoi, M.; Ono, Y.; Seto, M.; Kobayashi, Y.; Maeda, Y. *Solid State Commun.* **2001**, *120*, 165–170.

(8) (a) Fugita, W.; Awaga, K. *Science* **1999**, *286*, 261–262. (b) Fujita, W.; Awaga, K.; Matsuzaki, H.; Okamoto, H. *Phy. Rev. B.* **2002**, *65*, 064434(1−9).

(9) Shultz, D. A.; Fico, R. M.; Boyle, J. P. D.; Kampf, J. W. *J. Am. Chem. Soc.* **2001**, *123*, 10403–10404.

(10) (a) Itkis, M. E.; Chi, X.; Cordes, A. W.; Haddon, R. C. *Science* **2002**, *296*, 1443–1445. (b) Brusso, J. L.; Clements, O. P.; Haddon, R. C.; Itkis, M. E.; Leitch, A. A.; Okaly, R. T.; Reed, R. W.; Richardson, J. F. *J. Am. Chem. Soc.* **2004**, *126*, 8256–8265. (c) Brusso, J. L.; Clements, O. P.; Haddon, R. C.; Itkis, M. E.; Leitch, A. A.; Oakley, R. T.; Reed, R. W.; Richardson, J. F. *J. Am. Chem. Soc.* **2004**, *126*, 14692–14693.

Published on Web 09/15/2009

Bis-dithiolate metal ion-pair complexes have been actively studied for a long time as a wide range of conducting and magnetic materials as well as nonlinear optical materials.[11,12] Experimental and theoretical investigations indicated that the unusual physical properties in such kinds of ion-pair complexes originate from the intermolecular interactions of bis-dithiolate metal anions; as a result, the anionic stacking pattern strongly influences the physical properties of the materials. It is notable that the structural features of the countercation play an important role in tuning the stacking pattern of bis-dithiolate metal anions.[13−15] We have recently obtained a series of quasi-one-dimensional molecular materials that are $[Ni(mnt)_2]^-$-based (where mnt^{2-} = maleonitriledithiolate) with interesting magnetic behaviors, such as spin-Peierls-like transition, ferromagnetic ordering, and metamagnetic transformation, employing benzylpyridinium derivatives with λ-shaped and flexible molecular conformations to adjust the packing pattern of $[Ni(mnt)_2]^-$ anions in crystals.[13]

Most recently, we extended our previous studies of the series of $[Ni(mnt)_2]^-$ complexes and focused our research attention on $[Ni(dmit)_2]^-$ complexes,[16] because the $[Ni(dmit)_2]^-$ anion is the analog of $[Ni(mnt)_2]^-$ (both anions possess planar molecular geometry and delocalized electronic structure with $S = 1/2$ spin) and also is an excellent building block employed for the construction of molecular magnetic materials apart from its well-known electric conductivity.[14,15] In comparison with the $[Ni(mnt)_2]^-$ complex, the existence of versatile intermolecular S···S contacts in the crystal of the $[Ni(dmit)_2]^-$ complex (for example, head-to-head and lateral-to-lateral S···S contacts between $[Ni(dmit)_2]^-$ anions besides face-to-face S···S contacts often observed in the crystal of $[Ni(mnt)_2]^-$ complex could serve as valid cooperative effects in molecular magnetic or conducting materials) probably give hysteretic loops; on the other hand, the $[Ni(dmit)_2]^-$ complexes exhibit a rich polymorphism[14,15] (which can be defined as a chemical substance possessing at least two different arrangements in the crystalline solid state,[17,18] giving rise to materials with different physical properties).

Scheme 1. Molecular Structure of $[NO_2bzql][Ni(dmit)_2]$

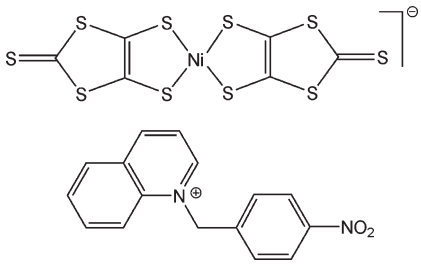

Herein, we report four ion-pair complexes of $[Ni(dmit)_2]^-$ with $[NO_2bzql]^+$ (NO_2bzql^+ = 1-(4-nitrobenzyl)quinolinium, and for its molecular structure, see Scheme 1). $[NO_2bzql][Ni(dmit)_2]$ (**1α** and **1*β***) and $[NO_2bzql][Ni(dmit)_2]\cdot CH_3COCH_3$ (**2α** and **2*β***) belong to two forms of polymorphs. Compounds **1α**, **1*β***, and **2α** exhibit magnetic bistability, and particularly, **1α** has a wide hysteretic loop around 55 K which, as far as we know, is a notably large thermal hysteresis loop for transition-metal-containing molecular materials, except for SC and cyano-bridged metal-to-metal charge-transfer-induced spin transition (CTIST) complexes.

Experimental section

Starting Materials and Chemicals. 4,5-Bis(thiobenzoyl)-1,3-dithiol-2-thione and $[NO_2bzql]Cl$ were prepared as described in the literature.[19,20] Other chemicals were purchased as analytical-grade reagents.

Powder Sample. To the suspended solution of 4,5-bis-(thiobenzoyl)-1,3-dithiol-2-thione (812 mg, 2.0 mmol) in dry methanol (20 mL) was added sodium (92 mg, 4.0 mmol) under a nitrogen atmosphere at room temperature. After all sodium balls disappeared, $NiCl_2\cdot 6H_2O$ (238 mg, 1 mmol) was added to the above-mentioned mixture with strong stirring for 20 min. I_2 (127 mg, 0.5 mmol) and $[NO_2bzql]Cl$ (1 mmol, 301 mg) in methanol were added in turn; the resulting dark blue powder was collected by filtration.

(11) (a) Nakamura, T.; Akutagawa, T.; Honda, K.; Vnderhils, A. E.; Coomber, A. T.; Friend, R. H. *Nature* **1998**, *394*, 159–162. (b) Malfant, I.; Andreu, R.; Lacroix, P. G.; Faulmann, C.; Cassoux, P. *Inorg. Chem.* **1998**, *37*, 3361–3370. (c) Kobayashi, A.; Fujiwara, E.; Kobayashi, H. *Chem. Rev.* **2004**, *104*, 5243–5246. (d) Kobayashi, H.; Cui, H. B.; Kobayashi, A. *Chem. Rev.* **2004**, *104*, 5265–5288. (e) Kato, R. *Chem. Rev.* **2004**, *104*, 5319–5346.

(12) (a) Staniland, S. S.; Fujita, W.; Umezono, Y.; Awaga, K.; Camp, P. J.; Clark, S. J.; Robertson, N. *Inorg. Chem.* **2005**, *44*, 546–551. (b) Dawe, L. N.; Miglioi, J.; Turnbow, L.; Taliaferro, M. L.; Shum, W. W.; Bagnato, J. D.; Zakharov, L. N.; Rheingold, A. L.; Arif, A. M.; Fourmigué, M.; Miller, J. S. *Inorg. Chem.* **2005**, *44*, 7530–7539. (c) Jeannin, O.; Clérac, R.; Fourmigué, M. *J. Am. Chem. Soc.* **2006**, *128*, 14649–14656. (d) Jeannin, O.; Clérac, R.; Fourmigué, M. *Chem. Mater.* **2007**, *19*, 5946–5954. (e) Nomura, M.; Fourmigué, M. *Inorg. Chem.* **2008**, *47*, 1301–1312.

(13) (a) Ren, X. M.; Meng, Q. J.; Song, Y.; Lu, C. S.; Hu, C. J.; Chen, X. Y.; Xue, Z. L. *Inorg. Chem.* **2002**, *41*, 5931–5933. (b) Ni, Z. P.; Ren, X. M.; Ma, J.; Xie, J. L.; Ni, C. L.; Chen, Z. D.; Meng, Q. J. *J. Am. Chem. Soc.* **2005**, *127*, 14330–14337. (c) Xie, J. L.; Ren, X. M.; Song, Y.; Zou, Y.; Meng, Q. J. *J. Chem. Soc., Dalton Trans.* **2002**, 2868–2872. (d) Xie, J. L.; Ren, X. M.; Gao, S.; Meng, Q. J. *Chem. Lett.* **2002**, *6*, 576–577. (e) Xie, J. L.; Ren, X. M.; Gao, S.; Zhang, W. W.; Li, Y. Z.; Lu, C. S.; Ni, C. L.; Liu, W. L.; Meng, Q. J.; Yao, Y. G. *Eur. J. Inorg. Chem.* **2003**, 2393–2396. (f) Xie, J. L.; Ren, X. M.; He, C.; Gao, Z. M.; Song, Y.; Meng, Q. J.; Kremer, R. K. *Chem. Phys. Lett.* **2003**, *369*, 41–48. (g) Xie, J. L.; Ren, X. M.; Song, Y.; Zhang, W. W.; Liu, W. L.; He, C.; Meng, Q. J. *Chem. Commun.* **2002**, 2346–2347. (h) Ren, X. M.; Meng, Q. J.; Song, Y.; Lu, C. S.; Hu, C. J.; Chen, X. Y. *Inorg. Chem.* **2002**, *41*, 5686–5692.

(14) (a) Clemenson, P. I. *Coord. Chem. Rev.* **1990**, *106*, 171–203. (b) Cassoux, P.; Valade, L.; Kobayashi, H.; Kobayashi, A.; Clark, R. A.; Underhill, A. E. *Coord. Chem. Rev.* **1991**, *110*, 115–160. (c) Cassoux, P. *Coord. Chem. Rev.* **1999**, *185−186*, 213–132. (d) Kobayashi, H.; Sato, A.; Tanaka, H.; Kobayashi, A.; Cassoux, P. *Coord. Chem. Rev.* **1999**, *190−192*, 921–932. (e) Ward, M. D.; McCleverty, J. A. *J. Chem. Soc., Dalton. Trans.* **2002**, 93–127. (f) Akutagawa, T.; Nakamura, T. *Coord. Chem. Rev.* **2000**, *198*, 297–311. (g) Akutagawa, T.; Nakamura, T. *Coord. Chem. Rev.* **2002**, *226*, 3–9. (h) Robertson, N.; Cronin, L. *Coord. Chem. Rev.* **2002**, *227*, 93–127.

(15) (a) Akutagawa, T.; Shitagami, K.; Nishihara, S.; Takeda, S.; Hasegawa, T.; Nakamura, T.; Hosokoshi, Y.; Inoue, K.; Ikeuchi, S.; Miyazaki, Y.; Saito, K. *J. Am. Chem. Soc.* **2005**, *127*, 4397–4402. (b) Akutagawa, T.; Hasegawa, T.; Nakamura, T.; Inabe, T. *J. Am. Chem. Soc.* **2002**, *124*, 8903–8911. (c) Nishihara, S.; Akutagawa, T.; Hasegawa, T.; Nakamura, T. *Chem. Commun.* **2002**, 408–409. (d) Akutagawa, T.; Hasegawa, T.; Nakamura, T.; Takeda, S.; Inabe, T.; Sugiura, K.; Sakata, Y.; Underhill, A. E. *Chem.—Eur. J.* **2001**, *7*, 4902–4912.

(16) Chen, Y. C.; Liu, G. X.; Song, Y.; Xu, H.; Ren, X. M.; Meng, Q. J. *Polyhedron* **2005**, *24*, 2269–2273.

(17) (a) Fettouhi, M.; Ouahab, L.; Hagiwara, M.; Codjovi, E.; Kahn, O.; Constant-Machado, H.; Varret, F. *Inorg. Chem.* **1995**, *34*, 4152–4159. (b) Laukhina, E.; Vidal-Gancedo, J.; Laukhin, V.; Veciana, J.; Chuev, I.; Tkacheva, V.; Wurst, K.; Rovira, C. *J. Am. Chem. Soc.* **2003**, *125*, 3948–3953. (c) Alberola, A.; Clements, O. P.; Collis, R. J.; Cubbitt, L.; Grant, C. M.; Less, R. J.; Oakley, R. T.; Rawson, J. M.; Reed, R. W.; Robertson, C. M. *Cryst. Growth Des.* **2008**, *8*, 155–161.

(18) (a) Kazmaier, P. M.; Hoffmannt, R. *J. Am. Chem. Soc.* **1994**, *116*, 9684–9691. (b) Zykova-Timan, T.; Raiteri, P.; Parrinello, M. *J. Phys. Chem. B* **2008**, *112*, 13231–13237.

(19) Wang, C. S.; Batsanov, A. S.; Bryce, M. R.; Howard, J. A. K. *Synthesis* **1998**, 1615–1618.

(20) Bulgarevich, S. B.; Bern, D. V.; Movshovic, D. Y.; Finocchiaro, P.; Failla, S. *J. Mol. Struct.* **1994**, *317*, 147–155.

The addition of 20 mL of acetone to the saturated acetone solution (10 mL) of the above powdered sample gave a dilute solution. Evaporation of such a dilute solution of the above powdered sample in acetone at room temperature over 1−2 weeks gave rise to needle-shaped **1α** as a single phase in the bottom of the beaker. Evaporation of the acetone/isopropyl alcohol, acetonitrile/isopropyl alcohol, or acetonitrile dilute solutions of the powdered sample all gave **1α** as a single phase. Elem anal. calcd for $C_{22}H_{13}N_2O_2S_{10}Ni$ (**1α**): C, 36.87; H, 1.83; N, 3.91%. Found: C, 36.87; H, 1.65; N, 4.10%. IR: absent $\nu_{C=O\ (acetone)}$ vibration band.

The **1*β*** phase was obtained through the heating of **2α** (see below) at 120 °C for 10−30 min. Elem anal. (%) calcd for $C_{22}H_{13}N_2O_2S_{10}Ni$ (**1*β***): C, 36.87; H, 1.83; N, 3.91. Found: C, 37.02; H, 1.47; N, 4.08. IR: absent $\nu_{C=O\ (acetone)}$ vibration band.

The **2α**-phase was obtained through the evaporation of the saturated solution (10 mL) of the above powdered sample in acetone over 1−2 weeks, gaving rhombus-shaped **2α** as a single phase in the bottom of the beaker. Elem anal. (%) calcd for $C_{25}H_{19}N_2O_3S_{10}Ni$ (**2α**): C, 38.76; H, 2.47; N, 3.62. Found: C, 38.88; H, 2.13; N, 3.70. IR: $\nu_{C=O(acetone)} = 1702\ cm^{-1}$.

Block **2*β*** could be obtained as a single phase from the wall of the beaker by quick evaporation of the saturated solution (10 mL) of the powder sample in acetone. Elem anal. (%) calcd for $C_{25}H_{19}N_2O_3S_{10}Ni$ (**2*β***): C, 38.76; H, 2.47; N, 3.62. Found: C, 38.76; H, 2.23; N, 3.71. IR: $\nu_{C=O(acetone)} = 1690\ cm^{-1}$.

Detailed IR spectra, thermogravimetric analysis, and XRD patterns for the four phases can be found in Figures S1, S2, and S3 (Supporting Information).

Physical Measurements. Elemental analyses for C, H, and N were performed on a Perkin-Elmer 240C elemental analyzer. IR spectra were collected on a VECTOR 22 spectrometer (KBr disk). Thermal analyses were carried out in a TGA V5.1A Dupont 2100 instrument from room temperature to 500 °C with a heating rate of 10 °C/min in the air. Powder X-ray diffraction patterns were recorded on a RigakuD/max-RA rotating anode X-ray diffractometer with graphite monochromatic Cu Kα (λ = 1.542 Å) radiation at room temperature. Variable-temperature magnetic susceptibility data were collected on microcrystalline samples from 2 to 300 K under a magnetic field of 2000 Oe, using a Quantum Design MPMS-XL SQUID magnetometer, and diamagnetic correction for each compound was estimated from Pascal's constants.[21]

Calculation Details. All density functional theory (DFT) calculations were carried out utilizing the Gaussian 98 program.[22] The whole nonmodelized molecular structures of the real complex **2α** in high-temperature (HT) and low-temperature (LT) phases were taken directly from X-ray crystallography complete structures, and calculations for magnetic exchange constants J were performed at the BPW91 level with the basis sets of LANL2DZ. The convergence criterion of SCF is 10^{-8}.

The interaction between two spins $\vec{S}_1$ and $\vec{S}_2$ can be described with the Heisenberg−Dirac−van Vleck Hamiltonian:[23−25]

$$\hat{H} = -2J\vec{S}_1\vec{S}_2 \quad (1)$$

where J is the magnetic exchange constant between $\vec{S}_1$ and $\vec{S}_2$. Assuming the so-called "weak bonding" regime, Noodleman et al.[26−28] evaluated J values within a broken symmetry framework using

$$J^{(1)} = \frac{E_{BS} - E_T}{S^2_{max}} \quad (2)$$

where E_{BS} and E_T denote the total energies in the broken symmetry (BS) singlet state and the triplet state, respectively, and S_{max} corresponds to the total spin of the high-spin state. It has been suggested that the following expression might give more reasonable solutions in the strong overlap region:[29,30]

$$J^{(2)} = \frac{E_{BS} - E_T}{S_{max}(S_{max}+1)} \quad (3)$$

However, Yamaguchi et al. claimed that J obtained by the approximate spin projection procedure reproduces the characteristic feature of J in the whole region:[31−33]

$$J^{(3)} = \frac{E_{BS} - E_T}{\langle S^2\rangle_T - \langle S^2\rangle_{BS}} \quad (4)$$

where $\langle S^2\rangle_T$ and $\langle S^2\rangle_{BS}$ denote the total spin angular momentum of the triplet state and broken-symmetry singlet state, respectively. Thus, the $J^{(3)}$ values obtained from eq 4 are employed in the following discussion.

X-Ray Crystallography. Single-crystal X-ray diffraction data were collected on a Bruker SMART APEX CCD diffractometer using graphite-monochromatized Mo Kα radiation (λ = 0.71073 Å) at 293 K for **1α**, at 293 K and 50 K for **2α**; and at 293 K for **2*β***. Lorentz polarization and absorption corrections were applied. The structures were solved by direct methods and refined with the full-matrix least-squares technique using the SHELXS-97 and SHELXL-97 programs.[34] Anisotropic thermal parameters were assigned to all non-hydrogen atoms. The crystallographic data and selected bond lengths for **1α**, **2α**, and **2*β*** are listed in Table 1 and Table S1 (Supporting Information). It was not possible to collect the single-crystal X-ray diffraction data for **1α** in the low-temperature phase owing to the single crystal being severely cracked, even though the crystal was cooled very slowly.

Results and Discussion

Complex 1α at 293 K. Complex **1α** crystallizes in monoclinic space group $P2_1/c$, and its asymmetric unit

(21) Boudreaux, E. A.; Mulay, L. N. *Theory and Applications of Molecular Paramagnetism*; John Wily & Sons: New York, 1976.
(22) Frisch, M. J.; Trucks, G. W.; Schlegel, H. B.; Scuseria, G. E.; Robb, M. A.; Cheeseman, J. R.; Zakrzewski, V. G.; Montgomery, J. A.; Stratmann, R. E., Jr.; Burant, J. C.; Dapprich, S.; Millam, J. M.; Daniels, A. D.; Kudin, K. N.; Strain, M. C.; Farkas, O.; Tomasi, J.; Barone, V.; Cossi, M.; Cammi, R.; Mennucci, B.; Pomelli, C.; Adamo, C.; Clifford, S.; Ochterski, J.; Petersson, G. A.; Ayala, P. Y.; Cui, Q.; Morokuma, K.; Salvador, P.; Dannenberg, J. J.; Malick, D. K.; Rabuck, A. D.; Raghavachari, K.; Foresman, J. B.; Cioslowski, J.; Ortiz, J. V.; Baboul, A. G.; Stefanov, B. B.; Liu, G.; Liashenko, A.; Piskorz, P.; Komaromi, I.; Gomperts, R.; Martin, R. L.; Fox, D. J.; Keith, T.; Al-Laham, M. A.; Peng, C. Y.; Nanayakkara, A.; Challacombe, M.; Gill, P. M. W.; Johnson, B.; Chen, W.; Wong, M. W.; Andres, J. L.; Gonzalez, C.; Head-Gordon, M.; Replogle, E. S.; Pople, J. A. *Gaussian 98*, revision A.11; Gaussian, Inc., Pittsburgh, PA, 2001.
(23) Heisenberg, W. *Z. Phys.* **1928**, *49*, 619–636.
(24) Dirac, P. A. M. *The Principles of Quantum Mechanics*; Clarendon Press: Oxford, U. K., 1947.
(25) Van Vleck, J. H. *The Theory of Electric and Magnetic Susceptibilities*; Oxford University Press: Oxford, U. K., 1932.
(26) Ginsberg, A. P. *J. Am. Chem. Soc.* **1980**, *102*, 111–117.
(27) Noodleman, L. *J. Chem. Phys.* **1981**, *74*, 5737–5743.
(28) Noodleman, L.; Davidson, E. R. *Chem. Phys.* **1986**, *109*, 131–143.
(29) Bencini, A.; Totti, F.; Daul, C. A.; Doclo, K.; Fantucci, P.; Barone, V. *Inorg. Chem.* **1997**, *36*, 5022–5030.
(30) Ruiz, E.; Cano, J.; Alvarez, S.; Alemany, P. *J. Comput. Chem.* **1999**, *20*, 1391–1400.
(31) Nagao, H.; Nishino, M.; Shigeta, Y.; Soda, T.; Kitagawa, Y.; Onishi, T.; Yoshioka, Y.; Yamaguchi, K. *Coord. Chem. Rev.* **2000**, *198*, 265–295.
(32) Soda, T.; Kitagawa, Y.; Onishi, T.; Takano, Y.; Shigeta, Y.; Nagao, H.; Yoshioka, Y.; Yamaguchi, K. *Chem. Phys. Lett.* **2000**, *319*, 223–230.
(33) Takano, Y.; Kitagawa, Y.; Onishi, T.; Yoshioka, Y.; Yamaguchi, K.; Koga, N.; Iwamura, H. *J. Am. Chem. Soc.* **2002**, *124*, 450–461.
(34) Sheldrick, G. M. *SHELXL-97*; University of Göttingen: Göttingen, Germany, 1997.

contains one anion together with one cation, as depicted in Figure 1. The anion shows an approximated planar geometry, and its bond lengths and angles are comparable

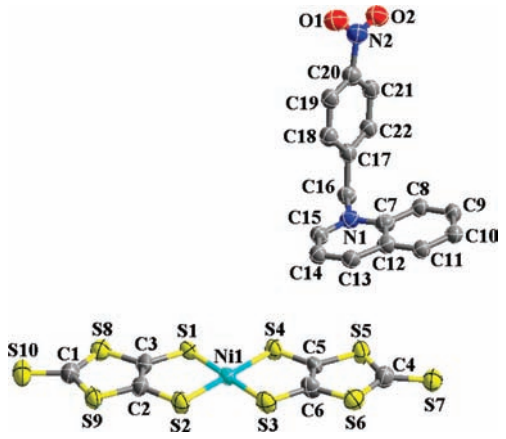

Figure 1. Molecular structure of **1α**.

to the reported $[Ni(dmit)_2]^-$ complexes.[14,15] The cation $[NO_2bzql]^+$ exhibits a λ-shaped conformation with an 88.50° dihedral angle between benzene and quinoline rings, which is similar to the reported benzylpyridinium derivatives. Neighboring cations form a molecular layer via weak intermolecular hydrogen bonds as well as van der Waals forces (please see Figure 2 and Figure S4, Supporting Information). The π-type dimers of $[Ni(dmit)_2]^-$ anions (the atom-to-atom distances: 3.643 Å for S5···C13, 3.492 Å for S6···N1, 3.570 Å for C2···C10, 3.342 Å for C4···C15, and 3.659 Å for C3···C9), which are filled in the channels formed by the cations, aligned through lateral S···S interactions to give a 2D supramolecular structure (Figure 2).

Complex 1β. Complex **1β** was only obtained as a powder through heating of **2α**. Its composition was verified by element analyses, IR spectra, and TG analyses (see Supporting Information). The DSC measurements of **2α** showed the existence of a phase transition following the loss of the acetone molecules (Figure S5). The XRD

Table 1. Crystallographic Data and Refinement Parameters for **1α**, **2α**, and **2β**

	1α	**2α**		**2β**
temp (K)	293	293 (HT)	50 (LT)	293
empirical formula	$C_{22}H_{13}N_2NiO_2S_{10}$	$C_{25}H_{19}N_2NiO_3S_{10}$	$C_{25}H_{19}N_2NiO_3S_{10}$	$C_{25}H_{19}N_2NiO_3S_{10}$
fw	716.65	774.73	774.73	774.73
cryst syst	monoclinic	triclinic	triclinic	monoclinic
space group	$P2_1/c$	$P\bar{1}$	$P\bar{1}$	$P2_1/n$
a (Å)	17.496(4)	8.026(2)	7.337(3)	12.219(3)
b (Å)	10.956(3)	12.499(4)	13.616(5)	8.134(2)
c (Å)	14.690(4)	16.496(5)	15.137(5)	31.928(8)
α (deg)		106.482(5)	106.398(6)	
β (deg)	99.611(5)	102.477(5)	95.967(6)	98.855(4)
γ (deg)		92.807(5)	91.973(7)	
V (Å^3)	2776.3(12)	1538.5(8)	1439.6(8)	3135.6(13)
Z	4	2	2	4
ρ (g cm^{-1})	1.715	1.672	1.787	1.641
F(000)	1452	790	790	1580
goodness of fit on F^2	1.052	1.098	1.048	1.081
R_1, $wR_2{}^a$ [$I > 2\sigma$(I)]	0.0528, 0.1379	0.0566, 0.1328	0.0411, 0.1127	0.0565, 0.1295
R_1, $wR_2{}^a$ [all data]	0.0651, 0.1414	0.0791, 0.1392	0.0554, 0.1162	0.0802, 0.1367

^{a} $R_1 = \sum||F_o| - |F_c||/|F_o|$, $wR_2 = [\sum w(\sum F_o{}^2 - F_c{}^2)^2/\sum w(F_o{}^2)^2]^{1/2}$.

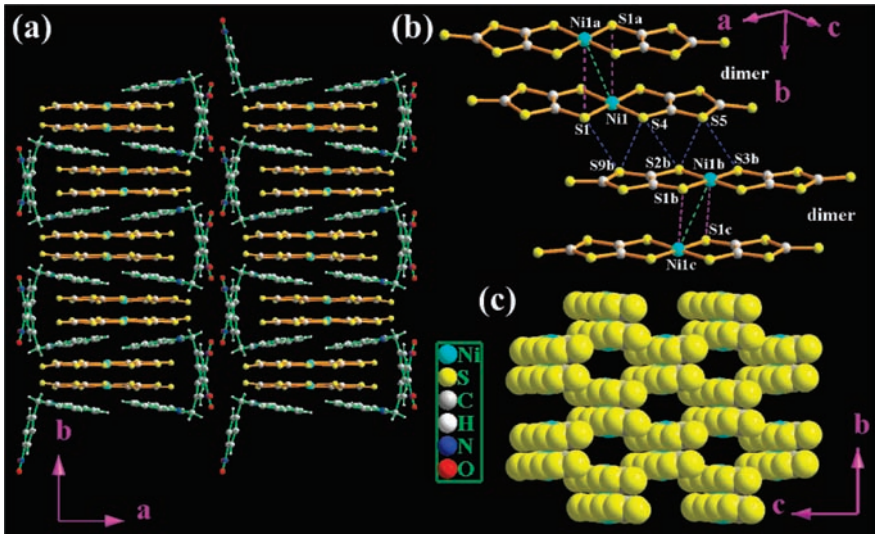

Figure 2. (a) Packing of **1α** viewed along c axis (b) Intra- and interdimer S···S and S···Ni contacts of the $[Ni(dmit)_2]^-$ anion: 4.013 Å for Ni1···Ni1a, 3.985 Å for Ni1···S1a, 3.663 Å for S1···S9b, 3.514 Å for S4···S9b, 3.554 Å for S4···S2b, 3.438 Å for S5···S2b, and 3.608 Å for S5···S3b (c) 2D supramolecular structure of $[Ni(dmit)_2]^-$ anions through S···S contacts in **1α**.

pattern (Figure S3, Supporting Information) further confirmed that it is a new phase different from the **1α** and **2α** phases. Further work is in progress to establish the cell parameters and space group for **1*β***, with the aim of solving its crystal and molecular structure.

Complex 2α at 293 K and 50 K. The crystal of **2α** belongs to the triclinic system with space group $P\bar{1}$ in both the HT phase (293 K) and the LT phase (50 K), and an asymmetric unit is comprised of one $[NO_2bzql]^+$ cation and one $[Ni(dmit)_2]^-$ ion together with one acetone molecule (Figure 3). The bond parameters for the planar anion and the cation are similar to those in **1α**. The cations build staircase-like columns along [011] via weak $\pi\cdots\pi$ interactions between two quinoline rings as well as hydrogen bond interactions between cations and acetone molecules (Figure 4a). The $[Ni(dmit)_2]^-$ dimers link into one-dimensional (1D) zigzag chains along [100] through intermolecular lateral S···S interactions (Figure 4), and such anionic chains fill in the cavity formed by the cation columns. In comparison with the HT phase, the structural distinctions for **2α** in the LT phase involve the following aspects: (1) The dihedral angle between benzene and the quinoline rings is 77.8° at 293 K versus 70.4° at 50 K. (2) Within the $[Ni(dmit)_2]^-$ dimer, less shrinking is observed along the stack direction (the distance between mean molecular planes, defined via Ni and four coordination S atoms, only reduces by 0.113 Å), while obvious slippage is found along the long molecular axis of the $[Ni(dmit)_2]^-$ anion (which is reflected in the Ni···Ni distance reducing from 3.966 Å in the HT phase to 3.535 Å in the LT phase), and such a slippage results in the two anions being nearly completely eclipsed in the LT phase (Figure 4b). (3) The interdimer interactions (including both terminal and lateral along [100] and [011] as mentioned above in the HT phase) are also strengthened at LT (please see Table 2).

Complex 2*β* at 293 K. Although **2*β*** and **2α** take the same stoichiometry of $[NO_2bzql][Ni(dmit)_2]\cdot CH_3COCH_3$ (see Figure S7, Supporting Information), the crystal symmetry of **2*β*** ($P2_1/n$) was higher than that of **2α** ($P\bar{1}$), and the arrangement of cations and anions in the two

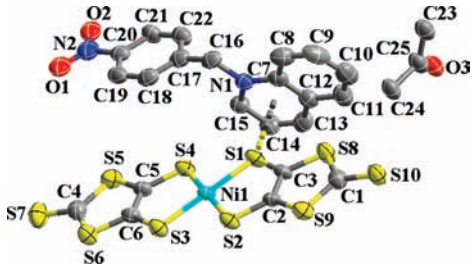

Figure 3. An asymmetric unit of **2α**.

Table 2. Ni···S and S···S Contacts (Å) in **2α** at HT and LT phases

atoms		lengths	
		HT	LT
Intradimer (face to face)			
Ni1	Ni1a	3.966	3.535
Ni1a	S3a	3.575	
S4	S2a		3.536
S3	S1a		3.554
S5	S9a		3.601
S6	S8a		3.657
Interdimer (lateral to lateral)			
S6	S9b	3.731	3.685
S3	S9b	3.700	3.537
S3	S2b	3.615	3.498
S2	S2b	3.601	3.379
Interdimer (head to head)			
S7	S10'		3.477

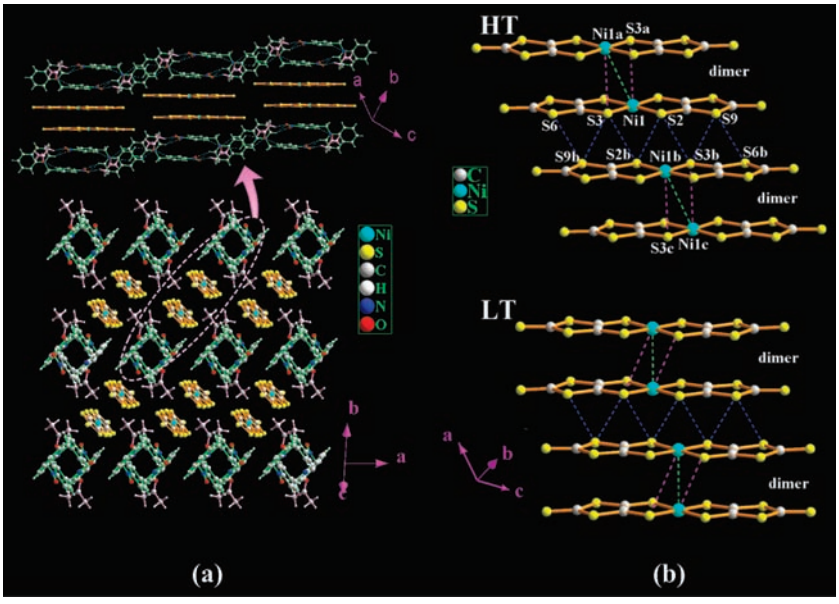

Figure 4. (a) Top: the packing fashion of **2α** along [011] at 293 K. Cations form stair-step columns, and anions lie between these cation columns. Bottom: the packing fashion of **2α** along [100] at 293 K. Anions form zigzag chains along [100]. NO_2bzql^+ cations, $[Ni(dmit)_2]^-$ anions, and acetone molecules are marked green, orange, and pink, respectively; hydrogen bonds are represented as blue dotted lines. (b) Intra- and interdimer S···S, S···Ni, and Ni···Ni contacts in **2α** along [100] at (top) 293 K and (bottom) 50 K.

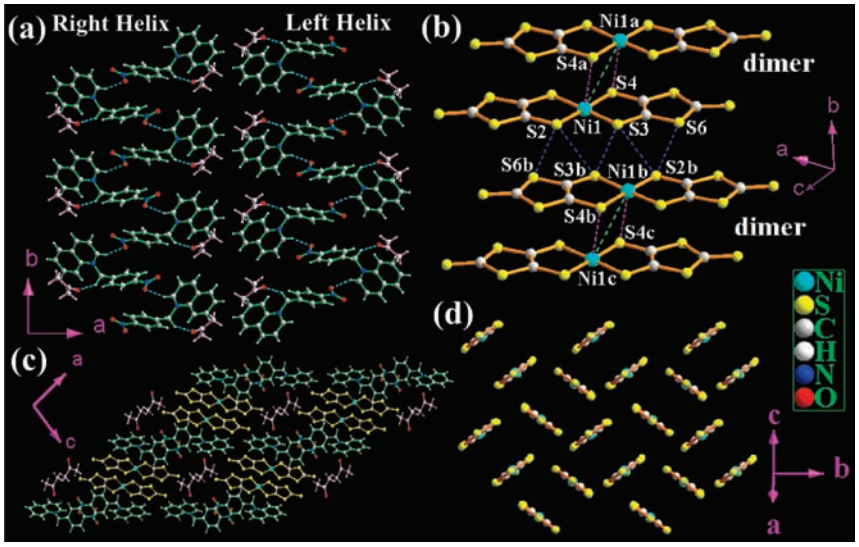

Figure 5. (a) Cations are linked into both right- and left-handed helices via hydrogen bonds (cations and acetone molecules marked as green and pink for clarity). (b) Side view of the $[Ni(dmit)_2]^-$ anion stack in **2*β*** with $d_{Ni1\cdots Ni1a}$ = 3.979 Å, $d_{Ni1\cdots S4a}$ = 3.732 Å, $d_{S2\cdots S6b}$ = 3.669 Å, $d_{S2\cdots S3b}$ = 3.661 Å, $d_{S3\cdots S3b}$ = 3.530 Å, $d_{S3\cdots S2b}$ = 3.661 Å, and $d_{S6\cdots S2b}$ = 3.669 Å (c). Anion arrangement with two orientations in **2*β***.

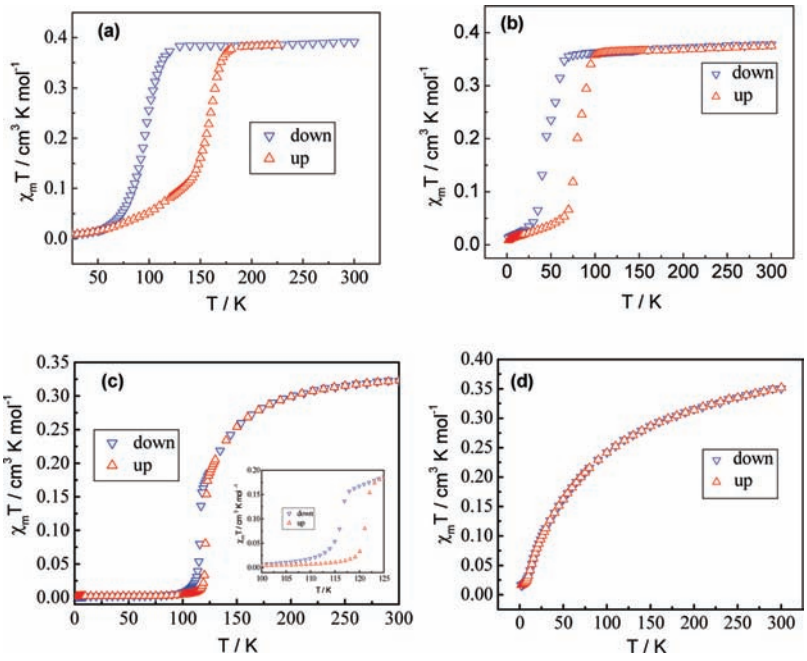

Figure 6. Plots of $\chi_m T$ versus T for (a) **1α**, (b) **1*β***, (c) **2α**, and (d) **2*β***.

crystals was also quite different. In **2*β***, benzene and quinoline rings form a dihedral angle of 84.43° (versus 77.8° in **2α**), and the cations form supramolecular helical chains with alternative right- and left-handed helices via weak hydrogen bonds with a C15#1···O2 distance of 3.237(7) Å (symmetry code: #1 = $1-x, 1/2+y, -1/2-z$; Figure 5). Acetone molecules are suspended alongside the cation helical chains through hydrogen bonds with a C16···O3 distance of 3.395(5) Å. Anion dimers are located in the pores of cations and acetone through $\pi\cdots\pi$ interactions (Figure 5c; the atom-to-atom distances: S1···C14, 3.654; S4···C13, 3.497; S4···C12, 3.597; C9···C16, 3.696 Å) and form a 1D chain along [010] through lateral-to-lateral S···S interactions (Figure 5b). In **2α**, the $[Ni(dmit)_2]^-$ anions are all parallel to each other, while in **2*β***, there are two $[Ni(dmit)_2]^-$ plane orientations with a dihedral angel of 72.5°(Figure 5d).

Magnetic Properties. Figure 6a−d show the temperature dependence of $\chi_M T$ of **1α**, **1*β***, **2α**, and **2*β***. At room temperature, the $\chi_M T$ value is 0.380 cm^3 K mol^{-1} for **1α**, which is close to the spin-only value for the $S = 1/2$ spin system. Upon cooling, the $\chi_M T$ value remains nearly constant to 130 K, drops quickly around 112 K, and reaches 0.015 cm^3 K mol^{-1} at 55 K. The warming mode reveals the occurrence of thermal hysteresis with an approximated 55 K loop. Complex **1*β*** exhibits similar magnetic bistability behavior with a ca. 30 K loop and lower critical temperatures (cooling $T_{down} \approx 70$ K and warming $T_{up} \approx 100$ K). Weakly antiferromagnetic (AFM) coupling behavior is observed for **2α** in the

300−120 K range, and a magnetic transition occurs around 100 K in the cooling process with a ca. 8 K loop (Figure 6c), while **2*β*** exhibits the AFM coupling feature without magnetic transition in the temperature range 2−300 K (Figure 6d). Bistable materials with a wide hysteretic loop are rarely observed in the dithiolate Ni complexes; as far as we known, only smaller hysteretic loops, ∼9 K for $[Me_4N][Ni(tfadt)_2]$ and ∼1 K and ∼10 K have been reported for **α** and ***β*** phases of $[H_2DABCO][Ni(mnt)_2]_2$.[35] Additionally, bis-dithiolate Ni complexes with the countercation $Fe(Cp^*)_2$ show thermal hysteresis.[36] Bistable materials with a hysteresis loop derived from the spin crossover of Fe^{3+} using Ni dithiolate as counterions were also reported.[37] As far as we know, the thermal hysteresis loop with a width of ∼55 K is a notably large for transition-metal-containing molecular materials, except for SC and cyano-bridged metal-to-metal CTIST complexes.

In the LT-phase, temperature-dependent magnetic susceptibilities show a thermally activated character for **1α**, **1*β***, and **2α**, indicating the existence of a spin gap (see Figure S8, Supporting Information). The magnetic susceptibilities of **1α** (in 2−96 K range), **1*β*** (in 2−55 K range), and **2α** (in 2−100 K range) are better described by eq 1:[38,39]

$$\chi_m = \frac{\alpha}{T^{\gamma_0}} \exp(-\Delta/k_B T) + \frac{C}{T} + \chi_0 \qquad (1)$$

where α is a constant corresponding to the dispersion of the excitation energy, Δ/k_B is the magnitude of the spin gap, γ_0 is a constant ($\gamma_0 = 0.5$), and the C/T term represents the contribution from magnetic impurities. Simulations gave the following results: $\alpha = 1.52$, $\Delta/k_B = 476$ K, $C = 4.38 \times 10^{-3}$ cm^3 K mol^{-1}, and $\chi_0 = 1.8 \times 10^{-4}$ cm^3·mol^{-1} for **1α**; $\alpha = 1.68$, $\Delta/k_B = 432$ K, $C = 7.81 \times 10^{-3}$ cm^3 K mol^{-1}, and $\chi_0 = 6.3 \times 10^{-4}$ cm^3 mol^{-1} for **1*β***; $\alpha = 1.49$, $\Delta/k_B = 816$ K, $C = 1.62 \times 10^{-3}$ cm^3 K mol^{-1}, and $\chi_0 = 2.0 \times 10^{-5}$ cm^3 mol^{-1} for **2α**.

The crystal structure data of **1α**, **1*β***, and **2α** in HT phases disclosed that the manners of anionic arrangement are similar to each other; namely, two face-to-face $[Ni(dmit)_2]^-$ anions form a π-type dimer, and the adjacent dimers are linked into a 1D zigzag chain through intermolecular lateral S···S interactions. On the other hand, **2α** loses solvent molecules from the lattice to give **1*β***, and it is reasonable to assume the existence of a similar anionic arrangement in **2α** and **1*β***. From the above analyses, the magnetic exchange model for a dimer or a Heisenberg alternating chain with $S = 1/2$ could be used to simulate

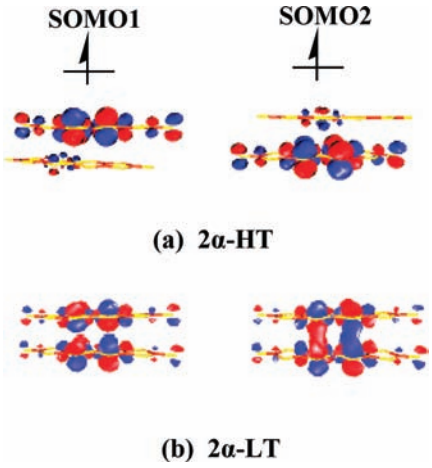

Figure 7. SOMOs of (a) **2α-HT** and (b) **2α-LT** calculated by UBPW91/LANL2DZ in the triplet state.

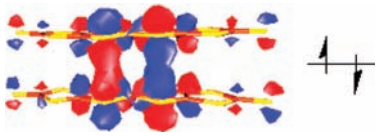

Figure 8. HOMO of **2α-LT** obtained by UBPW91/LANA2DZ in the BS state.

the temperature dependences of magnetic susceptibility for **1α**, **1*β***, and **2α** in HT phases as well as for **2*β*** over the entire temperature range (2−300 K). The fits revealed that both the dimer and Heisenberg alternating chain models with $S = 1/2$ cannot yield reasonable parameters for **1*β*** and **2*β***, while the isolated dimer model with $S = 1/2$ is described quite well and explains the magnetic behavior of **1α** and **2α** in HT phases, which gives rise to the energy gap between the singlet and triplet states at 46 K with a fixed g factor = 2 in the temperature range of 120−300 K for **1α** versus 168 K with a fixed g factor = 2 in the temperature range of 154−300 K for **2α** (see Figure S8, Supporting Information). Obviously, the AFM interaction within an intradimer is greatly enhanced from the HT phase to the LT phase owing to the improved π−π overlap.

Theoretical Calculations. To get a deeper understanding of the relationship between the anionic stacking pattern and magnetic coupling nature, the magnetic coupling constant J in the spin dimer has been calculated with the broken-symmetry approach using a DFT theoretical framework for **2α-HT** and **2α-LT**, and the Kohn−Sham type of SOMOs in the triplet states are displayed in Figure 7, which show two unpaired electrons almost localized in each monomer of the dimer in **2α-HT** but delocalized over the dimeric pair owing to two monomers getting closer in **2α-LT**. Such a delocalization picture is also clearly shown in the HOMO of **2α-LT** (Figure 8). Further, the calculated parameters in both the paramagnetic and nonmagnetic states are respectively given below: $\langle S^2\rangle_{BS} = 0.9277$, $\langle S^2\rangle_T = 2.0030$, and $J = -48.31$ cm^{-1}; $\langle S^2\rangle_{BS} = 0.0$, $\langle S^2\rangle_T = 2.0031$, and $J = -1518.18$ cm^{-1}, and these results are in qualitative agreement with the analyses of the temperature-dependent magnetic susceptibility in both HT and LT phases. Now, it is clear that the origin of the magnetic transition

(35) (a) Ren, X. M.; Akutagawa, T.; Nishihara, S.; Nakamura, T.; Fujita, W.; Awaga, K. *J. Phys. Chem. B* **2005**, *109*, 16610–16615. (b) Ren, X. M.; Nishihara, S.; Akutagawa, T.; Noro, S.; Nakamura, T. *Inorg. Chem.* **2006**, *45*, 2229–2234. (c) Ren, X. M.; Nishihara, S.; Akutagawa, T.; Noro, S.; Nakamura, T.; Fujita, W.; Awaga, K. *Chem. Phys. Lett.* **2006**, *418*, 423–427.

(36) Mochida, T.; Koinuma, T.; Akasaka, T.; Sato, M.; Nishio, Y.; Kajita, K.; Mori, H. *Chem.—Eur. J.* **2007**, *13*, 1872–1881.

(37) (a) Dorbes, S.; Valade, L.; Real, J.; Faulmann, C. *Chem. Commun* **2005**, 69–71. (b) Faulmann, C.; Jacob, K.; Dorbes, S.; Lampert, S.; Malfant, I.; Doublet, M.-L.; Valade, L.; Real, J. A. *Inorg. Chem.* **2007**, *46*, 8548–8559.

(38) Johnston, D. C.; Kremer, R. K.; Troyer, M.; Wang, X.; Klümper, A.; Bud'ko, S. L.; Panchula, A. F.; Canfield, P. C. *Phys. Rev. B* **2000**, *61*, 9558–9606.

(39) Troyer, M.; Tsunetsugu, H.; Wurtz, D. *Phys. Rev. B* **1994**, *50*, 13515–13527.

occurs in the $[Ni(dmit)_2]^-$ polymorphs; that is, upon cooling, the lattices shrink nonuniformly to enhance the π-orbital overlap of the $[Ni(dmit)_2]^-$ anions in a dimer, which induces a magnetic transition from a paramagnetic state to a nonmagnetic state.

Concluding Remarks

This work presented the crystal structures and magnetic properties for four $[Ni(dmit)_2]^-$-based pseudo-polymorphs. Combined the experimental data and theoretical analysis results, the following conclusions could be made: (1) The magnetic coupling nature between $[Ni(dmit)_2]^-$ anions is sensitive to the stacking pattern. Also, for a face-to-face stacked $[Ni(dmit)_2]^-$ dimer, there exists a weak AFM coupling interaction in a slippage pattern due to less π-orbital overlapping, while there is a stronger AFM coupling interaction in an eclipsed fashion owing to greater π-orbital overlapping. (2) The countercation with a flexible molecular conformation is favored to build a tunable crystal environment where the reorientation of $[Ni(dmit)_2]^-$ anions is easily achieved via intermolecular slippage upon cooling that is a requirement for a paramagnetic state to nonmagnetic state transition. Additionally, since these kinds of complexes often act as the charge carrier for molecular conductors, they are also promising in the investigation of potential electromagnetic bifunctional switches.

Acknowledgment. This work was financially supported by the National Basic Research Program of China (2007CB925102), National Nature Science Foundation of China (Grant No. 20490218), Jiangsu Science and Technology Department, and the Center of Analysis and Determining of Nanjing University.

Supporting Information Available: Additional figures and tables and crystallographic data for all complexes in CIF format can be obtained free of charge via the Internet at http://pubs.acs.org.